First-principles study of phonons and related ground-state properties and spectra in Zn-IV-N_2 compounds

Tula R. Paudel and Walter R. L. Lambrecht
Department of Physics, Case Western Reserve University, Cleveland, Ohio 44106-7079, USA
(Received 21 July 2008; published 18 September 2008)

The Zn-IV-N_2 compounds, with the group-IV element Si, Ge, and Sn, which have a common crystal structure closely related to the wurtzite-structure form a series analogous to the group-III nitrides GaN, AlN, and InN, respectively. Calculations of the phonons and related quantities in these materials are reported here using the density-functional perturbation-theory linear-response approach in the local-density approximation and using a plane-wave pseudopotential method. We focus on spectra, such as the imaginary part of the dielectric function and the energy-loss function as measurable by infrared absorption or reflectivity, and the Raman spectra. We also present phonon densities of states, band dispersions, and related integrated thermodynamic quantities such as the specific heat, and Helmholtz free energy and entropy as functions of temperature. Structural and elastic properties such as the lattice constants and bulk moduli are also reported. Finally, high-frequency and static dielectric tensors are presented. The trends in the series and the relation to the corresponding III-N nitrides are discussed. It is found that the bimodal bond-length distribution with IV-N bonds shorter than the Zn-N bonds (even for Sn) strongly modifies the spectra from those in III-N nitrides. While in $ZnGeN_2$ and $ZnSnN_2$ folded acoustic-like modes are clearly separated from the optic type modes, this is not the case in $ZnSiN_2$. The calculated Born effective charges indicate that $ZnGeN_2$ has the lowest ionicity of the three materials.

DOI: 10.1103/PhysRevB.78.115204 PACS number(s): 63.20.D−, 78.30.Fs

I. INTRODUCTION

The Zn-IV-N_2 group of compounds with the group-IV elements Si, Ge, and Sn forms a series analogous to the well-known III-N nitrides AlN, GaN, and InN but have, in comparison with the latter, only received very little study. Their close analogy to the III-N compounds makes them promising materials for the same types of wide-band-gap semiconductor applications, mainly in optoelectronics, but possibly also as host for dilute magnetic semiconductors,[1] or piezoelectric and nonlinear optical materials. The ternary nature of these compounds provides additional band-structure engineering opportunities because both the group-IV and group-II elements can be modified. Furthermore, these materials may share some of the properties of other II-IV-V_2 chalcopyrites in exhibiting a more complex defect physics, which could open new routes to doping control.

The crystal structures are closely related to those of the III nitrides as discussed in more detail in Sec. III A. The electronic properties are also closely related to the corresponding III nitrides but are not yet well established. Starting from $ZnGeN_2$, which is most directly related to GaN because Zn and Ge are in the same row of the periodic table as Ga, we find indeed that $ZnGeN_2$ has a band gap (3.40 eV excitonic band gap at 4 K from photoluminescence) (Ref. 2) close to that of GaN [3.483 band-gap free exciton (*A* exciton) at 4.2 K].[3] Earlier results by Larson *et al.*[4] gave a band-gap estimate of 2.67 eV for $ZnGeN_2$, but this estimate is probably referring to subband-gap defect absorption. Kikkawa and Morisaka[5] gave 3.1 eV from the direct optical-absorption edge. For $ZnSiN_2$ only one of the two cations is in an earlier row, so one expects the gap to be in between that of AlN (6.2 eV) and GaN. Endo *et al.*[6] reported an indirect absorption edge at 3.64 eV. Osinsky *et al.*[7] reported a gap of 4.46 eV for $ZnSiN_2$ based on optical transmittance. For $ZnSnN_2$ one expects a gap between that of GaN and InN (0.7 eV).[8] Our local-density approximation (LDA) band-structure calculations of $ZnGeN_2$, $ZnSiN_2$, and $ZnSnN_2$ will be discussed elsewhere.[9] Here, we only mention that using a full-potential linearized muffin-tin orbital (FP-LMTO) method, we obtain LDA gaps of 3.48 (indirect) and 3.69 eV (direct) for $ZnSiN_2$, 2.06 eV for $ZnGeN_2$, and 0.07 eV for $ZnSnN_2$. This means our band gap is underestimated by 1.34 eV for $ZnGeN_2$. LDA calculations using a similar FP-LMTO method gave 1.935 eV or an underestimate of 1.54 eV for GaN,[10] 4.255 eV or an underestimate of 1.95 eV for AlN, and 0.064 eV or an underestimate of 0.64 eV for InN. We thus see that the LDA underestimate is larger for the wider gap materials. This means we can expect a gap correction for $ZnSiN_2$ of at least 1.34 eV. This would give an estimated lower limit of the gap of 4.8 eV for $ZnSiN_2$. Making the plausible assumption that the gap correction is the average of that of $ZnGeN_2$ and that of AlN, we obtain an estimate of 5.1 eV. The calculations do predict a slightly smaller direct than indirect gap but the two are quite close. However, it indicates that the 3.64 eV value for the indirect gap[6] is not really the indirect gap but probably an underestimate because of subband-gap defect absorption. For $ZnSnN_2$, we may expect a gap correction between that of InN and that of $ZnGeN_2$ or a gap of about 1.0 eV. In any case, this indicates that the gaps in the $ZnSnN_2$, $ZnGeN_2$, and $ZnSiN_2$ span a wide range from the infrared to the ultraviolet. There have been a few previous LDA calculations[11–13] but firm conclusions on the gaps were not reached in those works because of the usual LDA underestimated of the gap. Similar values were obtained for the LDA gaps as ours.

In the present paper, we focus on the ground-state and phonon related properties of these materials. This paper con-

tinues our previously reported work on $ZnGeN_2$ (Refs. 14 and 15) and $ZnSiN_2$ (Ref. 16) by expanding the study to $ZnSnN_2$ and discussing the trends in the series. $ZnSnN_2$, to the best of our knowledge, has not yet been synthesized, so our work is completely predictive for this hypothetical compound. We focus on infrared absorption and Raman spectra because they are more readily applicable to small crystals. In fact infrared reflectance data for $ZnSiN_2$ were reported by Mintairov *et al.*[17] and analyzed by us in Ref. 16. Raman data for $ZnGeN_2$ were reported for $ZnGeN_2$ polycrystalline powders by Viennois *et al.*[18] and tentatively interpreted in Ref. 14. A Raman study on single-crystal $ZnGeN_2$ was presented in Ref. 15. Full phonon-dispersion curves are only measurable by neutron diffraction or inelastic x-ray scattering, which requires large single crystals. However, they are still an important part of a full understanding of the phonons in a material, so we present calculated dispersions along the high-symmetry lines in the Brillouin zone mostly to connect them with the density of phonon states. The latter have more practical importance because in defective materials, crystal momentum conservation may be relaxed and Raman spectra may then reflect density of phonon states. Once we have the density of phonon states, we can also calculate some thermodynamic quantities of interest, such as specific heat. In order to calculate LO-TO phonon splittings, the linear-response approach uses derivatives of the total energy versus a static electric field. The Born effective charges, which are key quantities in obtaining the LO-TO phonon splittings, also provide some information about the ionicity of the materials. Using the same derivatives, one obtains as a byproduct the high-frequency (but below band gap) dielectric tensor, giving us the indices of refraction by taking the square root. Experimental data on indices of refraction in $ZnSiN_2$ were reported by Cook *et al.*[19] The static dielectric constant is also obtained.

II. COMPUTATIONAL METHOD

The calculations were carried out using the linear-response approach[20–22] together with an iterative minimization norm-conserving pseudopotential plane-wave method[21–23] and within the framework of density-functional theory,[24,25] as implemented in the ABINIT package.[26] The density-functional perturbation theory is the basis of the linear-response approach. Once first-order perturbed wave functions are obtained, it allows one to obtain second-order derivatives of the energy versus atomic displacements, which give force constants; second derivatives versus a static electric field, giving susceptibilities $\chi_{\alpha,\beta}$ or dielectric tensors and mixed derivatives of the two, which give the Born effective charge tensor describing the LO-TO splittings. Using the $2n+1$ theorem, the first-order perturbed wave functions give the energy correct to third order so one can also calculate third derivatives. These allow one to calculate the Raman tensor elements from $\partial\chi_{\alpha\beta}/\partial\tau$, where τ is an atomic displacement. For further details on the calculation of the Raman matrix elements, we refer the reader to Veithen *et al.*,[27] and Deinzer and Strauch.[28] From the effective charges and the phonon eigenvectors, one obtains directly the oscillator strengths and hence the infrared-absorption spectra.[16]

The LDA was used for the exchange and correlation energies. In the Fritz-Haber pseudopotentials used,[29] the $3d$ electrons of Zn were treated as valence electrons. The calculations were carried out with a 70 Ry plane-wave energy cutoff, and the orthorhombic Brillouin zone was sampled with a regular and shifted $2\times2\times2$ k-point mesh. The phonon frequencies change by less then 1% when a plane-wave energy cut-off energy of 80 Ry and k-point mesh of $4\times4\times4$ is used, proving the results are well converged. Our criteria for self-consistency were changed by less than 10^{-22} Hartree^2 for the wave functions squared residual ($\langle\psi|(H-E)^2|\psi\rangle$ with $E=\langle\psi|H|\psi\rangle$), 10^{-6} Hartree for energies, and 10^{-6} Hartree/Bohr for forces. To obtain the phonon density of states, we used the approach described by Bungaro *et al.*[30] in which the phonons are calculated first on a coarse $2\times2\times2$ q-point mesh, the short-range force constants are obtained in real space by subtracting the known long-range behavior in q space followed by a Fourier transform, and the long-range forces are then added analytically when carrying out the calculations on a finer q-point integration mesh or for the points along symmetry lines.

III. RESULTS

A. Crystal structure and bulk moduli

The crystal structure of these compounds is a superstructure of the wurtzite structure with overall orthorhombic symmetry. In the idealized structure, the lattice basis vectors **a**, **b**, and **c** are related with wurtzite lattice vectors $\mathbf{a}^w$, $\mathbf{b}^w$, and $\mathbf{c}^w$ by $\mathbf{a}=2\mathbf{a}^w$, $\mathbf{b}=\mathbf{a}^w+2\mathbf{b}^w$, and $\mathbf{c}=\mathbf{c}^w$. Here the wurtzite $\mathbf{b}^w$ vector is at 120° from the $\mathbf{a}^w$ vector, both lying in the plane perpendicular to the $\mathbf{c}^w$ vector. Thus, the orthorhombic **b**

TABLE I. Calculated and experimental lattice parameters a, b, and c in amperes in Zn-IV-N_2 compounds.

Compound	Calculated			Experimental		
	a	b	c	a	b	c
$ZnSiN_2$ (Å) [a]	6.01	5.28	4.98	6.18	5.35	5.05
$ZnGeN_2$ (Å) [b]	6.33	5.36	5.11	6.44	5.45	5.19
$ZnSnN_2$ (Å)	6.76	5.85	5.58			

[a]Mintairov *et al.* (Ref. 17).
[b]Wintenberger *et al.* (Ref. 31).

TABLE II. Bulk moduli and their pressure derivative of Zn-IV-N_2 compounds.

Compound	B (GPa)	B'
$ZnSiN_2$	228	4.4
$ZnGeN_2$	197	4.4
$ZnSnN_2$	184	4.8

$=\sqrt{3}\mathbf{a}^w$ and is along what is sometimes called the orthohexagonal axis. We could call the superstructure a $2\times\sqrt{3}\times1$ superstructure. However, small distortions from this idealized structure occur, maintaining the orthorhombic symmetry.

The calculated lattice constants obtained by minimizing the energy using the ABINIT approach are in excellent agreement with the experimental lattice constants of $ZnSiN_2$ (Ref. 17) and $ZnGeN_2$.[31] Table I shows that the b/a ratios of $ZnSiN_2$, $ZnGeN_2$, and $ZnSnN_2$ are 1.73, 1.69, and 1.73, respectively, all close to $\sqrt{3}$ as expected. Similarly the c/a ratios of $ZnSiN_2$, $ZnGeN_2$, and $ZnSnN_2$ are 1.65, 1.61, and 1.65. The ideal wurtzite c/a ratio is $\sqrt{8/3}\approx1.633$, and that in GaN is 1.626. Thus the c/a is slightly smaller than ideal in the case of $ZnGeN_2$ and GaN while it is slightly larger than ideal in the case of $ZnSiN_2$ and $ZnSnN_2$, contrary to the cases of AlN ($c/a=1.602$) and InN ($c/a=1.615$).

As expected, the lattice constants increase and hence the bulk modulus, shown in Table II, decreases with the atomic number of the group-IV elements. The bulk moduli and their pressure derivatives were obtained by fitting the Vinet equation of state[32] to the energy versus volume curves. We also note that the calculated unit-cell volumes 158, 173, and 220 $Å^3$ for $ZnSiN_2$, $ZnGeN_2$, and $ZnSnN_2$, respectively, underestimate the experimental ones 167 and 182 Å for $ZnSiN_2$ and $ZnGeN_2$, respectively, by about 5%, which is usual for the LDA.

The atomic positions of each of the elements are not available experimentally except for $ZnGeN_2$.[31] We therefore tabulate the atomic position of each of anions and cations in Table III. There are two inequivalent N positions: one above the group-II atom and one above the group-IV atom. A figure of the structure can be found in Ref. 14. Relaxation shows that the cations essentially remain in the same positions while the nitrogen positions deviate from their ideal positions. The nitrogen atoms essentially find an optimized position in the tetrahedron of cations surrounding them by moving away from Zn and toward the group-IV element. The resulting average bond lengths are summarized in Table IV. The Zn-N bond length remains constant among the three compounds while the IV-N bond increases with the atomic radius of the group-IV element. This increment of the IV-N bond length causes the bond strength to decrease and may thus be expected to decrease the phonon frequencies corresponding to IV-N bond stretches. In $ZnSnN_2$ the two bond lengths are almost equal.

B. Phonons and related properties

Infrared absorption or reflectivity and Raman spectroscopy provide powerful tools to study the crystalline quality of new materials. They measure essentially the phonons at Γ because of crystal momentum conservation in a perfect crystal. However, if the presence of defects relaxes this conservation rule, the spectra rather correspond to density of phonon states integrated over the Brillouin zone. Therefore it is important to study the phonons at Γ as well as the density of states.

TABLE III. Atomic positions (reduced coordinates) in the unit cell.

Compounds	Atoms	x	y	z
$ZnSiN_2$	Zn	0.501	−0.003	−0.055
	Si	0	0.0123	0
	N^a_{Si}	0.027	0.028	0.343
	N_{Zn}	0.278	0.469	0.407
$ZnGeN_2$	Zn	0.5	0.0	0.0
	Ge	0.0	0.0	0.0
	N_{Ge}	0.017	0.019	0.356
	N_{Zn}	0.268	0.484	0.395
$ZnSnN_2$	Zn	0.5	−0.001	0
	Sn	0	0.011	0
	N_{Sn}	0.027	0.028	0.344
	N_{Zn}	0.278	0.474	0.406

1. Phonons at Γ

The phonons at the center of the Brillouin zone, the Γ point, are classified according to the irreducible representations of the point group C_{2v}. For a full discussion of the symmetry, see Peshek *et al.*[15] We briefly remark here that the irreducible representations a_1, b_1, and b_2 correspond to modes with the same symmetry as a vector along z, x, and y, respectively, where these are chosen along the c, a, and b axes of the crystal. These modes are infrared active and also are subject to an LO-TO splitting. That is, a static electric field in the x direction will affect the b_1 modes, and hence if we approach the Γ point from the x direction, the b_1^{LO} mode will be obtained. If we approach Γ from the y or z direction, the b_1^{TO} mode is obtained. For directions in between these orthogonal directions, a mixed mode will be obtained with a splitting in proportion to the x component of the wave vector. Similar considerations apply to the other infrared-active modes. The a_2 modes are antisymmetric under both mirror planes but symmetric under the twofold rotation along the c axis. They are not infrared active but Raman active. Since there are 16 atoms in the cell, there are in total 48 modes at

TABLE IV. Average bond lengths (in Å) in Zn-IV-N_2 compounds.

Compound	Zn-N	IV-N
$ZnSiN_2$	2.06	1.75
$ZnGeN_2$	2.02	1.83
$ZnSnN_2$	2.05	2.00

TABLE V. Phonon frequencies in $ZnSnN_2$ at the Γ point in cm^{-1}.

a_2	b_{1T}	b_{1L}	b_{2T}	b_{2L}	a_{1T}	a_{1L}
109	134	135	107	107	108	108
127	153	153	131	131	124	124
130	178	180	155	159	146	147
153	203	211	191	191	163	167
185	224	224	237	238	206	206
235	368	401	355	355	344	359
338	429	435	370	440	359	389
424	516	539	496	525	527	477
483	541	579	560	562	528	554
543	673	708	675	692	666	666
668	713	720	700	739	677	716
713						

any wave vector not counting the different limits that can be obtained at Γ. It turns out that there are 12 modes of each symmetry. The lowest TO modes of a_1, b_1, and b_2 symmetries at Γ correspond to a uniform translation of the crystal and have zero frequency.

Since the phonon frequencies at Γ for $ZnSiN_2$ and $ZnGeN_2$ were already given in Ref. 16 and 14, respectively, we here only give the values for $ZnSnN_2$ in Table V. In subsequent sections we present spectra related to these modes for all three materials for easy comparison.

2. Infrared spectra and related quantities

One of the most widely used methods to probe phonons is infrared absorption. The oscillator strength function of the infrared-active phonon mode is calculated from[22]

$$S_{n,\alpha\alpha} = \left| \sum_{\kappa} Z^*_{\kappa,\alpha\alpha} U_n(\kappa,\alpha) \right|^2, \tag{1}$$

with $Z^*_{\kappa,\alpha\alpha} = V \partial P_\alpha / \partial \tau_{\kappa\alpha}(\mathbf{q}=0)$ the Born effective charge tensor components, $U_n(\kappa,\alpha)$ the eigenvector for mode n, in which κ labels the atom, and α the Cartesian directions. P_α is the polarization, V the volume of the unit cell, τ_κ the position of the κth atom, and $\mathbf{q}=0$ indicates that a collective displacement of atoms is considered, the displacement being the same in every unit cell. The Born effective charges, also known as dynamic effective charges,[33] are associated with lattice vibration and are different from the static effective charges, which are related with the static transfer of charge form cation to anion in the formation of an ionic crystal compared to the free atoms. While both are in effect a measure of ionicity or polarity of the bonds, the dynamic effective charges are directly measurable through the LO-TO splitting. The orthorhombic symmetry of the system makes $Z^*_{\kappa.\alpha\alpha}$ diagonal and hence also the oscillator strength function. The Born effective charges are given in Table VI. Their sum over atoms for each direction satisfies the neutrality charge neutrality sum rule. For a_1, b_1, and b_2 modes, only z, x, and y components, respectively, of the oscillator strength are nonzero and only these modes contribute to the corresponding effective charge tensor element.

Table VI shows that the Born effective charges of the group-IV element and the nitrogen associated with it is larger in $ZnSiN_2$ and $ZnSnN_2$ than in $ZnGeN_2$ for each of the diagonal components. This trend is the same as for AlN, GaN, and InN,[30] where also the lowest dynamic charges are found for GaN. We did not observe any clear trend for the dynamic effective charge associated with Zn and its counterpart nitrogen. The average values for cations and anions are comparable to those in the corresponding III nitrides.

In terms of these oscillator strengths, the dielectric function is given by

$$\varepsilon_{\alpha\alpha}(\omega) = \varepsilon^{\infty}_{\alpha\alpha} + \frac{4\pi}{V} \sum_n \frac{S_{n,\alpha\alpha}}{\omega_n^2 - \omega^2 - i\Gamma_n \omega}, \tag{2}$$

where ω_n and Γ_n are the mode frequencies and damping factors, respectively. The high-frequency dielectric tensor, i.e., at frequencies below the band gap but well above the phonon modes, is given in Table VII. The value obtained in the static limit $\omega \to 0$ including the phonon contributions is also given.

TABLE VI. Born effective charge tensors.

Compound	Zn	IV	N_{IV}	N_{Zn}
		Z_{xx}		
$ZnSiN_2$	1.807	3.193	−2.519	−2.480
$ZnGeN_2$	1.809	3.159	−2.493	−2.475
$ZnSnN_2$	1.943	3.243	−2.612	−2.574
		Z_{yy}		
$ZnSiN_2$	1.785	3.345	−2.259	−2.870
$ZnGeN_2$	1.760	3.319	−2.275	−2.133
$ZnSnN_2$	1.912	3.368	−2.444	−2.836
		Z_{zz}		
$ZnSiN_2$	2.064	3.334	−2.991	−2.407
$ZnGeN_2$	2.028	3.329	−2.919	−2.447
$ZnSnN_2$	2.251	3.474	−3.077	−2.650

TABLE VII. High-frequency and static dielectric tensor components.

Compound	$\varepsilon_{xx}^{\infty}$	$\varepsilon_{yy}^{\infty}$	$\varepsilon_{zz}^{\infty}$	ε_{xx}^{0}	ε_{yy}^{0}	ε_{zz}^{0}
$ZnSiN_2$	4.842	4.867	5.290	8.704	9.278	10.015
$ZnGeN_2$	5.166	5.239	5.725	9.222	9.276	10.610
$ZnSnN_2$	5.853	5.931	7.239	11.151	11.895	15.088

The dielectric tensor components are seen to be increasing from $ZnSiN_2$ to $ZnSnN_2$. This is mostly because of the decreasing band gap, which is related primarily to the lower *s*-like conduction-band states of the group-IV cation. The higher the atomic number *Z* the more the *s*-like states feel the nucleus, and hence these states move down relative to the anion *p*-like states making up the valence band. A similar trend is observed in case of III-N such as AlN, GaN, and InN. By taking the square root of the high-frequency dielectric constants, we obtain the indices of refraction, given separately for convenience in Table VIII.

The peaks of the imaginary part of the frequency dependent dielectric function in the infrared range $\mathrm{Im}[\varepsilon(\omega)]$ correspond to the transverse optical modes, while the poles of the real part, $\mathrm{Re}[\varepsilon(\omega)]$, or the peaks in $\mathrm{Im}[-\varepsilon^{-1}(\omega)]$ (the loss function) correspond to the longitudinal optical phonon modes. These calculated spectra are shown in Fig. 1.

The trend of decreasing phonon frequencies with increasing atomic number of the group-IV element is clear for all modes. In part this trend is related to the mass of group-IV ion. However, the high-frequency modes primarily involve N atoms and the trend therefore also reflects the trend of decreasing bond strength, which in turn is related to the increase in IV-N bond lengths.

Next, we discuss the separation of the modes into folded acoustic and optical modes. In wurtzite we have six modes in the "optical range" and three folded acoustic modes. Of these six high-frequency modes, only three are optically active: the doubly degenerate E_1 and nondegenerate A_1 modes. The present materials have a four times larger unit cell, so the six modes in the optical range will give rise to 24 modes. Since all modes are equally divided over the four symmetries, we expect six modes of each optically active symmetry or a total of 18 modes. The lower five modes of each optically active symmetry are expected to have weak oscillator strengths because they correspond to folded acoustic type modes and are expected to occur in a well separated wave number range. This expectation is confirmed for $ZnGeN_2$ and $ZnSnN_2$ but not in $ZnSiN_2$. First of all, we do not see a separate range of five low-frequency modes in $ZnSiN_2$. This overlap of the folded acoustic and optic ranges is interesting but not entirely unexpected considering that also in AlN, the gap between acoustic and optical ranges is already quite small. The modes near the top of the acoustic range correspond to modes that are folded from the Brillouin-zone boundary in the parent compound and hence have primarily cation vibration character. The stretching out of this region is thus related to the lighter mass of the IV atom. Second, we can see that in $ZnGeN_2$ there is barely any spectral intensity at all below 400 cm^{-1}, corresponding to the five low-frequency modes. In $ZnSiN_2$ we can see a low-frequency peak near 300 cm^{-1} for the three symmetries. Interestingly this peak is also visible in $ZnSnN_2$ where it lies below 200 cm^{-1} although it is rather weak for the b_2 symmetry. So, one of the acoustic range phonons appears to have a moderately strong oscillator strength. Interestingly, this is stronger in the two materials with the larger Born effective charges, which is indicative of a higher ionicity. The higher six modes of each symmetry are seen to be the strongest and to also have the large LO-TO splitting as expected.

At present the only experimental information we have on these spectra is for the b_1 symmetry modes in $ZnSiN_2$.[17] It was discussed in Ref. 16. Fairly good although not perfect agreement was obtained in terms of both frequencies and oscillator strengths.

The a_2 modes are not visible in infrared spectroscopy. We show them in Fig. 2 for completeness' sake.

3. Raman Spectra

Another popular spectroscopy used to study phonons is Raman scattering. In first-order Raman spectroscopy, one obtains again essential information on the $\mathbf{q}=0$ phonons. However, other selection rules apply. In the present case, all modes are Raman active. However, which mode is active depends on the scattering geometry. A detailed discussion is provided in Ref. 15. The Raman intensity is proportional to $|\mathbf{e}_i \cdot \alpha^m \cdot \mathbf{e}_o|^2$, where $\mathbf{e}_i$ and $\mathbf{e}_o$ are the incident and scattered light polarization vectors and α is the second-rank Raman susceptibility tensor for mode m given by

$$\alpha_{\alpha\beta}^{m} = \sqrt{V} \sum_{\kappa\gamma} \frac{\partial \chi_{\alpha\beta}}{\partial \tau_{\kappa\gamma}} u_m(\kappa\gamma), \tag{3}$$

where $u_m(\kappa\gamma)$ is the eigenvector of mth mode. As can be seen it involves the derivatives of the susceptibility versus atomic displacements dotted into the mode's eigenvector. We can thus view it as the derivative of the susceptibility versus the amplitude of a collective atomic displacement pattern with the symmetry of mode m. The product representation of the irreducible representations of the incoming and outgoing polarization vectors must contain the irreducible representation of the vibrational mode in order to give a nonzero value.

TABLE VIII. Indices of refraction.

Compound	n_{xx}	n_{yy}	n_{zz}
$ZnSiN_2$	2.200	2.206	2.300
$ZnGeN_2$	2.273	2.289	2.393
$ZnSnN_2$	2.419	2.435	2.690

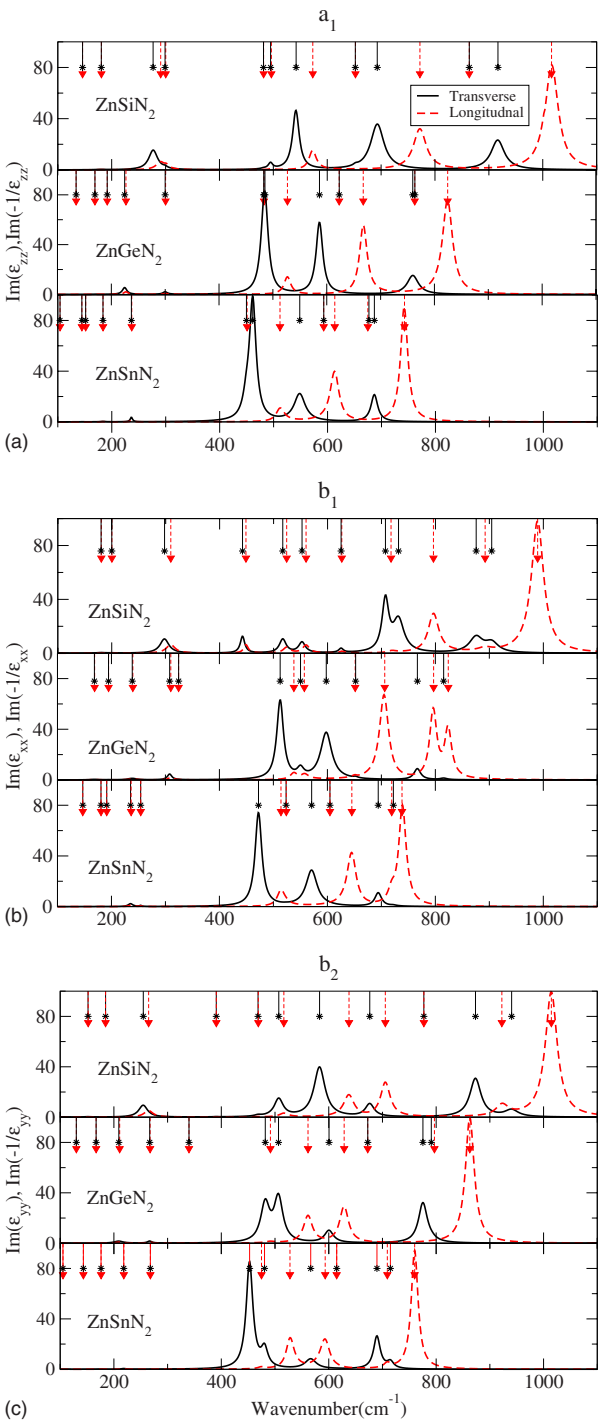

FIG. 1. (Color online) Infrared absorption spectra related to the modes at Γ for Zn-IV-N_2 compounds. The solid black lines give the Im[$\varepsilon(\omega)$], the dashed red lines give the loss function Im[$-\varepsilon^{-1}(\omega)$]. The three panels in each plot are for the group-IV elements Si, Ge, and Sn from top to bottom. The different plots correspond to the different infrared-active symmetries. The arrows at the top of each panel give the individual modes: shorter and longer arrows represent transverse and longitudinal phonon modes, respectively. Note that only 11 phonon modes are shown visible as the lowest one is the zero-frequency acoustic phonon mode. The spectra are calculated using Eq. (2) with a damping factor chosen between 5–30 cm^{-1} with increasing width for higher frequency modes, as suggested by the experimental data for $ZnSiN_2$ (Ref. 16).

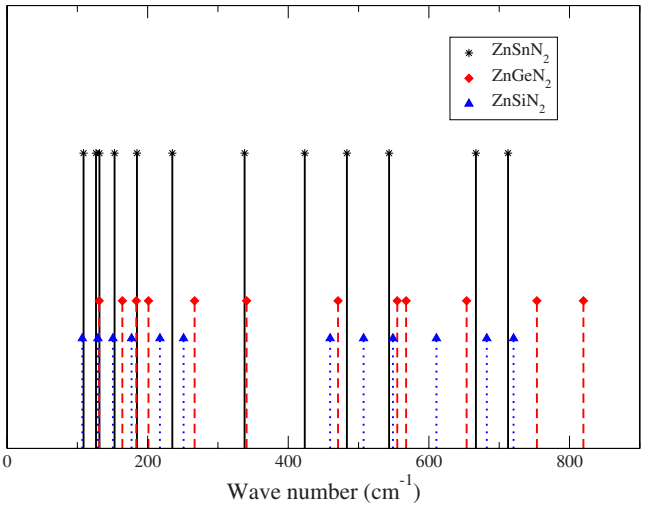

FIG. 2. (Color online) Comparison of the a_2 phonon modes of Zn-IV-N_2 compounds. The height of the arrows is chosen arbitrarily.

In this case, this means the Raman susceptibility tensor has the following form depending on the mode's symmetry. For a_1 symmetry we have

$$a_1:\begin{pmatrix} a & \cdot & \cdot \\ \cdot & b & \cdot \\ \cdot & \cdot & c \end{pmatrix}, \tag{4}$$

which means that incident and scattered light must have parallel polarization but different values will be obtained for the x, y, and z directions. The scattering geometry is fully specified by giving $\mathbf{k}_i(\mathbf{e}_i\mathbf{e}_o)\mathbf{k}_o$. If the wave vectors $\mathbf{k}_i$ and $\mathbf{k}_o$ are parallel to a vector corresponding to the mode's irreducible symmetry, then the longitudinal modes are excited, otherwise the transverse ones. For example, $z(xx)\bar{z}$ measures the a tensor component of the longitudinal a_{1L} modes because a_1 corresponds to z while $x(yy)\bar{x}$ will measure the b component of the a_{1T} modes. The remaining modes correspond to off-diagonal matrix elements of the Raman tensor as follows:

$$a_2:\begin{pmatrix} \cdot & d & \cdot \\ d & \cdot & \cdot \\ \cdot & \cdot & \cdot \end{pmatrix},\quad b_1:\begin{pmatrix} \cdot & \cdot & e \\ \cdot & \cdot & \cdot \\ e & \cdot & \cdot \end{pmatrix},\quad b_2:\begin{pmatrix} \cdot & \cdot & \cdot \\ \cdot & \cdot & f \\ \cdot & f & \cdot \end{pmatrix}. \tag{5}$$

The spectra corresponding to the transverse modes are shown in Figs. 3–6 using a fixed linewidth broadening of each mode. We organize the figures by symmetry mode and compare the different materials in each plot. We may note that the intensity of the a_1 components is an order of magnitude stronger than the other modes. They also appear significantly stronger in $ZnGeN_2$ than in the other materials. Experimental data are available only for $ZnGeN_2$ and were presented in Ref. 15. Good agreement was obtained in particular for the $c=\alpha_{zz}$ component of the a_{1T} modes. It was also found that the polarization dependence of these spectra is a sensitive measure of the crystalline quality and ordering in the material. Table IX provides the nonzero Raman tensor components for each mode and would allow the reader to recon-

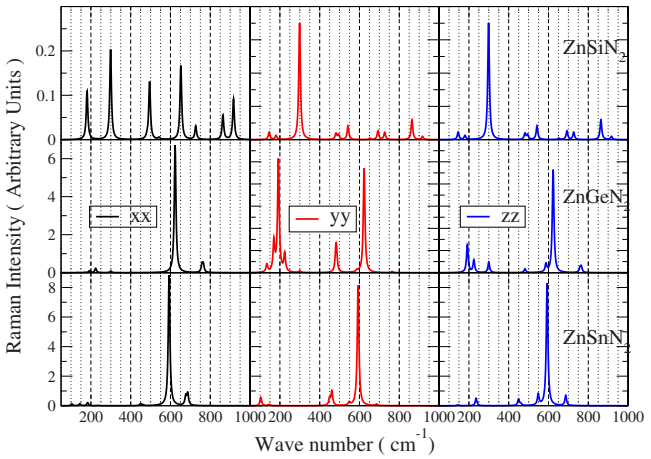

FIG. 3. (Color online) Calculated Raman spectra for modes of a_{1T} symmetry for the Zn-IV-N_2 compounds. Note that the peak intensities depend on the Raman tensor component as selected by the scattering geometry: xx is measured in $y(xx)\bar{y}$, yy in $x(yy)\bar{x}$, and zz in $\perp(zz)\bar{\perp}$ with $\perp$ any wave vector in the c plane.

struct simulated spectra for longitudinal modes and for other choices of the broadening factor. Comparing the equivalent symmetry modes in the different materials shows that the spectra are quite different. For example for $ZnGeN_2$ the strongest Raman peak is the a_{1T} peak at about 620 cm^{-1} in the zz component of the tensor. This same type of peak can be seen in $ZnSnN_2$ at slightly lower frequency. In $ZnSiN_2$, however, the strongest peak corresponds to a totally different mode near 300 cm^{-1}. Generally speaking, we can see more similarities between the spectra for $ZnGeN_2$ and $ZnSnN_2$. The Raman spectra show less clear trends than the infrared spectra.

4. Density of phonon states and phonon-dispersion curves

The density of phonon states integrated over the whole Brillouin zone is a quantity of fundamental interest because it determines several thermodynamic quantities. Furthermore, it also may prove useful in the interpretation of Raman spectra. In case of disordered materials or nanocrystalline materials, the crystal momentum conservation rules are not obeyed and the spectra have a closer resemblance to the density of states although some parts of the spectra could still have different weight than others. Also, second-order Raman spectroscopy often has a strong resemblance to density of states if pure harmonics dominate rather than sum frequencies of different modes.

The full phonon-dispersion curves along symmetry lines in the Brillouin zone in this material, which has a large unit cell and hence small zone, are rather complex because of the many foldings compared to the underlying wurtzite Brillouin zone. However, they are useful to compare with the density of states. Measurement of these phonon band structures requires neutron diffraction or high-resolution inelastic x-ray scattering and is only possible on large enough single crystals of high quality, which are not yet available for these materials.

The phonon dispersions along symmetry lines and the corresponding densities of states are shown in Figs. 7–9 for

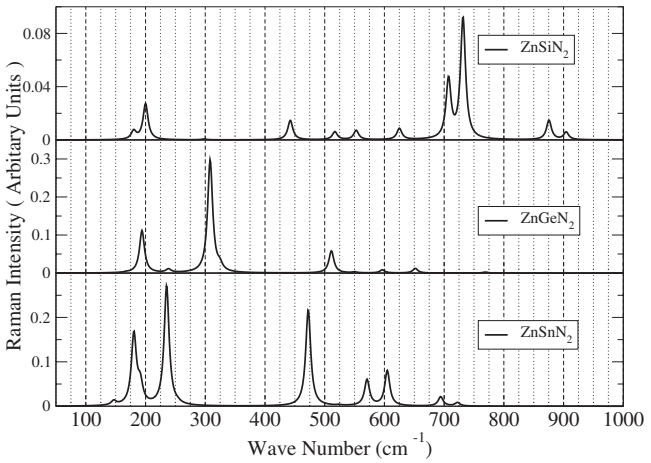

FIG. 4. Calculated Raman spectra for modes of b_{1T} symmetry for the Zn-IV-N_2 compounds. This component is measured in $y(zx)\bar{y}$ geometry.

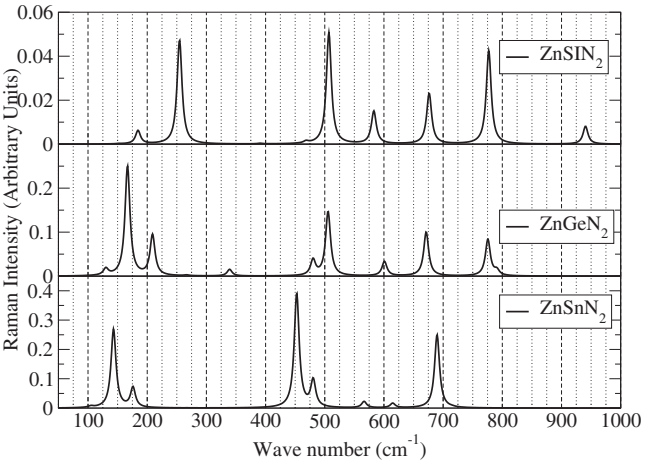

FIG. 5. Calculated Raman spectra for modes of b_{2T} symmetry for the Zn-IV-N_2 compounds. This component is measured in $x(zy)\bar{x}$ geometry.

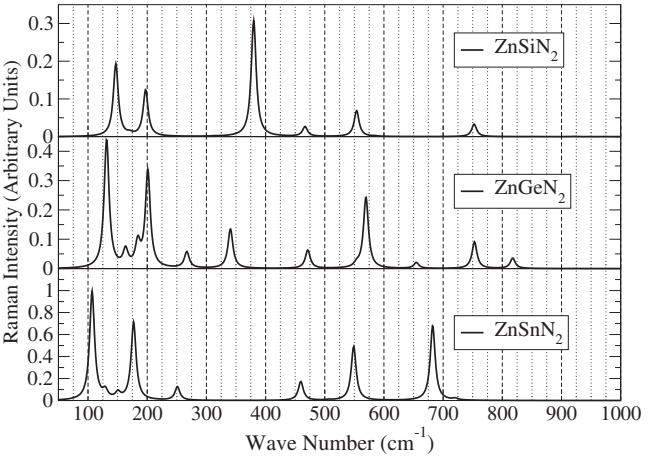

FIG. 6. Calculated Raman spectra for modes of a_2 symmetry for the Zn-IV-N_2 compounds. This component is measured in $z(xy)\bar{z}$ geometry.

TABLE IX. Raman tensor components for each of the modes.

Modes	$ZnSiN_2$			$ZnGeN_2$			$ZnSnN_2$		
	xx	*yy*	*zz*	*xx*	*yy*	*zz*	*xx*	*yy*	*zz*
a_1	$-1.22\ 10^{-5}$	$1.13\ 10^{-4}$	$1.13\ 10^{-4}$	$5.92\ 10^{-5}$	$-2.06\ 10^{-4}$	$-2.06\ 10^{-4}$	$3.05\ 10^{-4}$	$-3.86\ 10^{-4}$	$-3.79\ 10^{-5}$
	$3.13\ 10^{-4}$	$-1.04\ 10^{-4}$	$-1.04\ 10^{-4}$	$8.32\ 10^{-5}$	$-5.15\ 10^{-4}$	$-5.15\ 10^{-4}$	$-4.65\ 10^{-5}$	$1.13\ 10^{-5}$	$4.38\ 10^{-5}$
	$7.09\ 10^{-4}$	$6.01\ 10^{-4}$	$6.01\ 10^{-4}$	$-2.19\ 10^{-4}$	$-1.14\ 10^{-3}$	$-1.14\ 10^{-3}$	$2.49\ 10^{-4}$	$7.23\ 10^{-5}$	$-1.22\ 10^{-5}$
	$-7.15\ 10^{-4}$	$9.40\ 10^{-4}$	$9.40\ 10^{-4}$	$3.97\ 10^{-4}$	$5.30\ 10^{-4}$	$5.30\ 10^{-4}$	$2.93\ 10^{-4}$	$1.22\ 10^{-4}$	$5.54\ 10^{-4}$
	$1.70\ 10^{-4}$	$-3.51\ 10^{-4}$	$-3.51\ 10^{-4}$	$3.27\ 10^{-4}$	$2.21\ 10^{-4}$	$2.21\ 10^{-4}$	$3.80\ 10^{-4}$	$1.39\ 10^{-4}$	$7.13\ 10^{-4}$
	$-9.72\ 10^{-4}$	$-3.24\ 10^{-4}$	$-3.24\ 10^{-4}$	$-5.74\ 10^{-5}$	$1.34\ 10^{-3}$	$1.34\ 10^{-3}$	$-3.11\ 10^{-4}$	$-7.23\ 10^{-4}$	$-3.27\ 10^{-4}$
	$1.88\ 10^{-4}$	$-6.01\ 10^{-4}$	$-6.01\ 10^{-4}$	$-4.39\ 10^{-5}$	$-8.77\ 10^{-4}$	$-8.77\ 10^{-4}$	$-5.15\ 10^{-4}$	$1.82\ 10^{-3}$	$1.21\ 10^{-3}$
	$-1.48\ 10^{-3}$	$2.24\ 10^{-4}$	$2.24\ 10^{-4}$	$-5.96\ 10^{-5}$	$4.67\ 10^{-4}$	$4.67\ 10^{-4}$	$1.23\ 10^{-3}$	$2.83\ 10^{-3}$	$-1.60\ 10^{-4}$
	$-6.03\ 10^{-5}$	$-6.21\ 10^{-4}$	$-6.21\ 10^{-4}$	$-6.33\ 10^{-3}$	$-3.75\ 10^{-3}$	$-3.75\ 10^{-3}$	$-6.97\ 10^{-3}$	$-6.77\ 10^{-3}$	$-6.72\ 10^{-3}$
	$1.16\ 10^{-3}$	$1.21\ 10^{-3}$	$1.21\ 10^{-3}$	$-1.88\ 10^{-3}$	$-2.18\ 10^{-4}$	$-2.18\ 10^{-4}$	$4.71\ 10^{-3}$	$-2.11\ 10^{-4}$	$-3.07\ 10^{-4}$-
	$-1.59\ 10^{-3}$	$-5.13\ 10^{-4}$	$-5.13\ 10^{-4}$	$1.91\ 10^{-3}$	$4.72\ 10^{-4}$	$4.72\ 10^{-4}$	$-2.94\ 10^{-4}$	$-1.34\ 10^{-4}$	$-1.13\ 10^{-3}$
		xz=zx			*xz=zx*			*xz=zx*	
b_1		$-7.46\ 10^{-5}$			$-1.95\ 10^{-5}$			$-2.04\ 10^{-5}$	
		$-1.72\ 10^{-4}$			$2.40\ 10^{-4}$			$1.48\ 10^{-4}$	
		$-3.76\ 10^{-5}$			$8.36\ 10^{-5}$			$-1.33\ 10^{-4}$	
		$-2.89\ 10^{-4}$			$-6.31\ 10^{-4}$			$-6.57\ 10^{-4}$	
		$-2.18\ 10^{-4}$			$1.50\ 10^{-4}$			$-2.39\ 10^{-4}$	
		$2.53\ 10^{-4}$			$-4.76\ 10^{-4}$			$-7.29\ 10^{-4}$	
		$3.17\ 10^{-4}$			$-1.03\ 10^{-4}$			$-4.41\ 10^{-4}$	
		$-8.34\ 10^{-4}$			$2.10\ 10^{-4}$			$4.68\ 10^{-4}$	
		$1.24\ 10^{-3}$			$2.82\ 10^{-4}$			$-2.06\ 10^{-4}$	
		$6.06\ 10^{-4}$			$1.52\ 10^{-4}$			$2.48\ 10^{-4}$	
		$3.89\ 10^{-4}$			$-7.65\ 10^{-5}$			$3.86\ 10^{-4}$	
		yz=zy			*yz=zy*			*yz=zy*	
b_2		$8.88\ 10^{-6}$			$-5.89\ 10^{-5}$			$5.99\ 10^{-5}$	
		$7.52\ 10^{-5}$			$3.07\ 10^{-4}$			$1.88\ 10^{-4}$	
		$2.92\ 10^{-4}$			$-2.36\ 10^{-4}$			$8.65\ 10^{-6}$	
		$-3.35\ 10^{-5}$			$-3.97\ 10^{-5}$			$1.23\ 10^{-4}$	
		$7.54\ 10^{-5}$			$-1.56\ 10^{-4}$			$-9.95\ 10^{-5}$	
		$-6.22\ 10^{-4}$			$3.48\ 10^{-4}$			$-5.0\ 10^{-5}$	
		$-3.91\ 10^{-4}$			$-7.45\ 10^{-4}$			$1.40\ 10^{-3}$	
		$-5.73\ 10^{-4}$			$-4.24\ 10^{-4}$			$1.34\ 10^{-4}$	
		$-9.04\ 10^{-4}$			$8.37\ 10^{-4}$			$-4.95\ 10^{-4}$	
		$-1.54\ 10^{-5}$			$-8.92\ 10^{-4}$			$-1.23\ 10^{-3}$	
		$4.89\ 10^{-4}$			$3.37\ 10^{-4}$			$7.50\ 10^{-5}$	
		xy=yx			*xy=yx*			*xy=yx*	
a_2		$3.35\ 10^{-4}$			$4.53\ 10^{-4}$			$7.67\ 10^{-4}$	
		$6.23\ 10^{-5}$			$2.03\ 10^{-4}$			$1.43\ 10^{-4}$	
		$3.62\ 10^{-4}$			$-2.72\ 10^{-4}$			$1.78\ 10^{-4}$	
		$4.20\ 10^{-5}$			$6.04\ 10^{-4}$			$-4.13\ 10^{-4}$	
		$-1.13\ 10^{-3}$			$-3.30\ 10^{-4}$			$-5.88\ 10^{-5}$	
		$-4.06\ 10^{-4}$			$-6.66\ 10^{-4}$			$-3.69\ 10^{-4}$	
		$7.95\ 10^{-4}$			$6.39\ 10^{-4}$			$6.64\ 10^{-4}$	
		$-1.05\ 10^{-4}$			$3.25\ 10^{-4}$			$1.12\ 10^{-4}$	
		$-1.99\ 10^{-6}$			$-1.54\ 10^{-3}$			$-1.85\ 10^{-3}$	
		$7.70\ 10^{-4}$			$5.13\ 10^{-4}$			$4.94\ 10^{-4}$	
		$1.53\ 10^{-6}$			$-1.28\ 10^{-3}$			$-2.49\ 10^{-3}$	
		$-1.13\ 10^{-4}$			$8.71\ 10^{-4}$			$5.98\ 10^{-4}$	

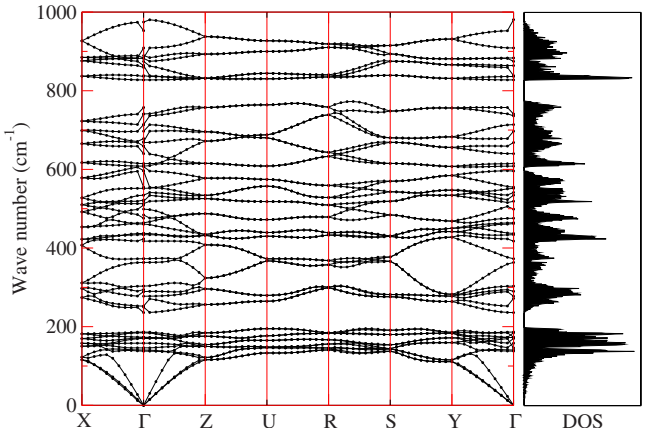

FIG. 7. (Color online) Phonon dispersions and density of states in $ZnSiN_2$.

$ZnSiN_2$, $ZnGeN_2$, and $ZnSnN_2$, respectively. For an easier comparison of the densities of states in the different materials, we collected them in Fig. 10.

The phonon-dispersion curves show some discontinuities at Γ. This is related to the nonanalytic behavior. We actually replace the modes at Γ with the correct ones for the wave vector approaching Γ in the direction shown, as discussed earlier. However, the mesh used for deriving the short-range force constants by Fourier transform is rather coarse, only a $2\times2\times2$ mesh. The phonons along the **q** points along the symmetry lines are obtained by Fourier transforming back these short-range force constants and adding the analytical form of the $\mathbf{q}\rightarrow0$ behavior. If the mesh is too coarse, this procedure may overestimate the contribution of the nonanalytical terms and hence overestimate the LO-TO splitting near Γ. Furthermore, the phonons at Γ were adjusted by insuring the sum rules on the effective charges.[22] Thus, we caution that the phonon curves may not be as accurate as the values at the Γ point. However, a finer Fourier transform mesh was too demanding for our currently available computer resources. The main purpose of showing the phonon dispersions here is to show their relation to the density of states and to show the overall topology. The small inaccuracies near Γ may thus be ignored.

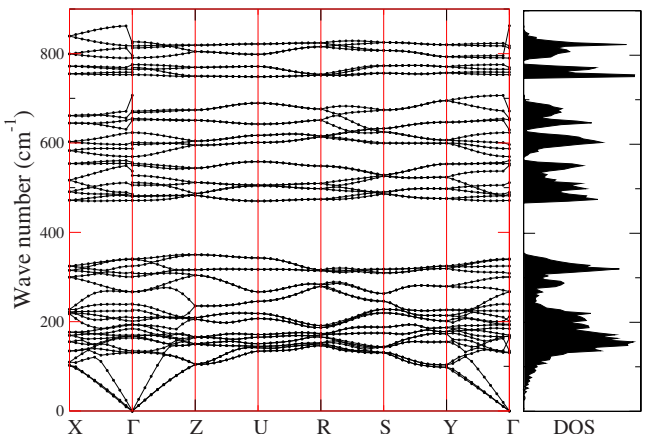

FIG. 8. (Color online) Phonon dispersions and density of states in $ZnGeN_2$.

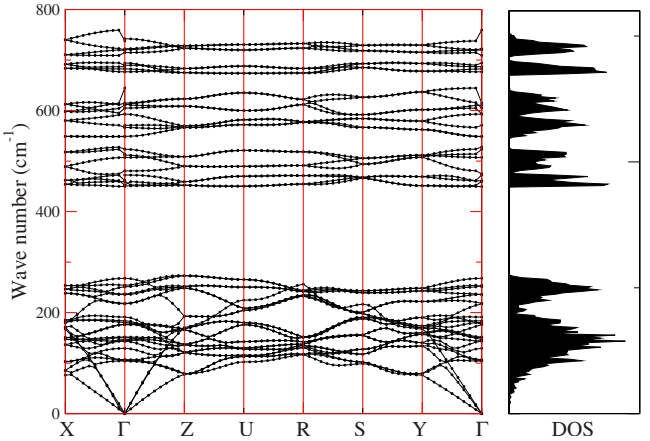

FIG. 9. (Color online) Phonon dispersions and density of states in $ZnSnN_2$.

We can see that the spectra have some similarities but also marked differences in the overall distribution of the phonons over the energy range. In $ZnSnN_2$ four separate branches separated by gaps can be distinguished. In $ZnGeN_2$, the lower "folded acoustic" band is considerably stretched to higher frequencies and the middle two bands have just touched. In $ZnSiN_2$ we see again that the acoustic and optical ranges have merged into one broad band.

As a rough guide, we can describe the nature of the vibrations as follows. The top of the acoustic bands corresponds to folded Brillouin-zone-edge modes dominated by the heaviest atoms, which would be Sn and Ge in $ZnSnN_2$ and $ZnGeN_2$, respectively, but Zn in $ZnSiN_2$. In $ZnGeN_2$ and $ZnSnN_2$, a total of 24 bands occur in this folded acoustic range. But for $ZnSiN_2$ there is only one peak in the DOS in this region and there are only 11 bands in this purely acoustic region. So clearly, the acoustic modes corresponding to Si motion are merged with the optic band. Returning to $ZnGeN_2$ and $ZnSnN_2$ two main peaks occur in what we could call the transverse optic region. They are clearly separated in $ZnSnN_2$. Inspection of some of the eigenvectors indicates that the lower peak may be dominated by Zn-N bonds and the upper region by Ge-N or Sn-N bonds. In fact,

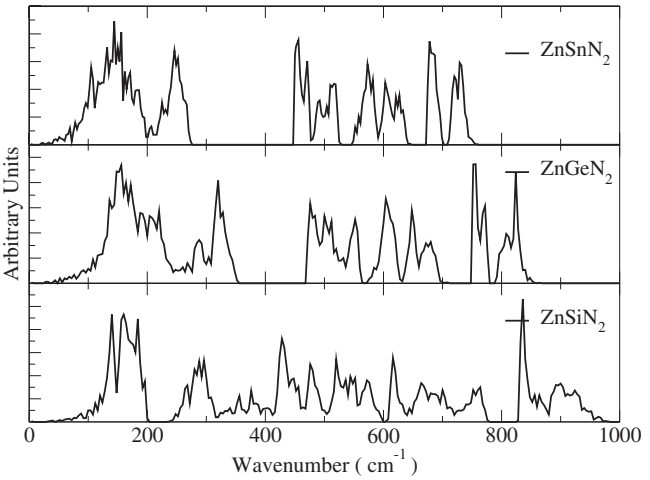

FIG. 10. Total density of state in Zn-IV-N_2 compounds.

the Zn-N bonds are longer and thus give weaker force constants, leading to lower frequencies. The highest modes correspond to the longitudinal branch and again are seen to be split in two peaks. For $ZnSiN_2$ it is more difficult to interpret the peaks. We caution however that all the modes show rather complex behavior. They are rather complex combinations of various types of bond stretches, bond bendings, etc. Some show predominant motion in the z direction, while others are dominated by intralayer bond stretches. In reality they are all rather mixed up.

We can also see that in $ZnSiN_2$ there is a strong peak at 300 cm^{-1}, which overlaps with the predicted TO peak in this range (see Fig. 1). As discussed in more detail in Ref. 16, this means that phonon-phonon scattering between the zone-center and zone-boundary modes may lead to a short phonon lifetime for such modes, and this may explain why such modes have not been observed. For $ZnSnN_2$ where these anomalously low TO modes occur at about 200 cm^{-1}, we also see that there will be a similar situation of overlap with a strong peak in density of states.

5. Thermodynamical Properties

As is well known, the contribution of the phonons to the thermodynamic quantities, such as the Helmholtz free energy ΔF, the energy $\Delta E = \partial(\beta \Delta F)/\beta$, the specific heat at constant volume $\Delta C_v = \partial \Delta E/\partial T$, and the entropy $\Delta S = (\Delta E - \Delta F)/T$ as a functions of temperature can all be expressed in terms of the density of states. Here $\beta = (k_B T)^{-1}$ with k_B as Boltzmann's constant. Following Lee *et al.*,[34] we define the density of states normalized as follows:

$$g(\omega) = \frac{1}{3nN} \sum_{\mathbf{q},l} \delta[\omega - \omega_l(\mathbf{q})], \tag{6}$$

in terms of the mode frequencies $\omega_l(\mathbf{q})$ and where n and N represents the number of atoms per unit cell and total number of the unit cells in the crystal. One obtains, per cell,

$$\Delta F = 3nk_B T \int_0^{\omega_m} \ln\left\{2 \sinh\frac{\hbar\omega}{2k_B T}\right\} g(\omega) d\omega,$$

$$\Delta E = 3n\frac{\hbar}{2} \int_0^{\omega_m} \omega \coth\left(\frac{\hbar\omega}{2k_B T}\right) g(\omega) d\omega,$$

$$\Delta C_v = 3nk_B \int_0^{\omega_m} \left(\frac{\hbar\omega}{2k_B T}\right)^2 \operatorname{csch}^2\left(\frac{\hbar\omega}{2k_B T}\right) g(\omega) d\omega, \tag{7}$$

in which ω_m is the maximum phonon frequency. These quantities as a function of temperature are shown in Figs. 11 and 12.

The variation in the free energy and internal energy with temperature is smaller in the case of $ZnSiN_2$, even though numerically the free energy and hence internal energy are the largest. Consequently the specific heat is smallest in case of $ZnSiN_2$. A similar trend is observed comparing with the specific-heat data of InN, GaN, and AlN by Davydov *et al.*,[35] Nipko *et al.*,[36] and Kosshchenko *et al.*[37] The specific-heat capacity approaches its classical value of 24.942 J/mol K at high temperature and reaches it approximately at 855 K in $ZnSnN_2$, 1019 K in $ZnGeN_2$, and 1133 in $ZnSiN_2$.

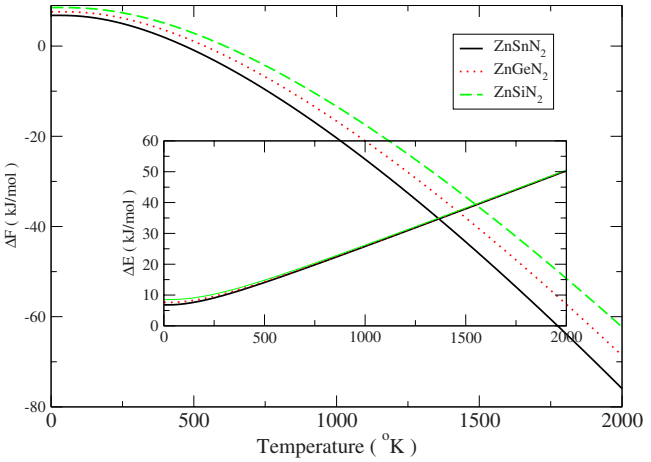

FIG. 11. (Color online) Helmholtz free energy and total energy (inset) of Zn-IV-N_2 compounds plotted against temperature.

At zero temperature, we obtain the zero-point energy

$$\Delta F_0 = \Delta E_0 = 3nN \int_0^{\omega_m} \frac{\hbar\omega}{2} g(\omega) d\omega. \tag{8}$$

The calculated zero-point energies of $ZnSiN_2$, $ZnGeN_2$, and $ZnSnN_2$ are 8.5, 7.6, and 6.1 kJ/mol, respectively.

IV. CONCLUSIONS

A comprehensive study of the ground-state structural properties and phonon related quantities in the Zn-IV-N_2 compounds was presented. These include (1) phonon modes at Γ, including the LO-TO splittings; (2) $\mathrm{Im}[\varepsilon(\omega)]$ corresponding to TO modes and $\mathrm{Im}[-\varepsilon^{-1}(\omega)]$ corresponding to LO modes as observable in infrared absorption or reflectivity; (3) calculated first-order Raman spectra including the Raman tensor matrix elements for each of the symmetry irreducible representations as measurable in different polariza-

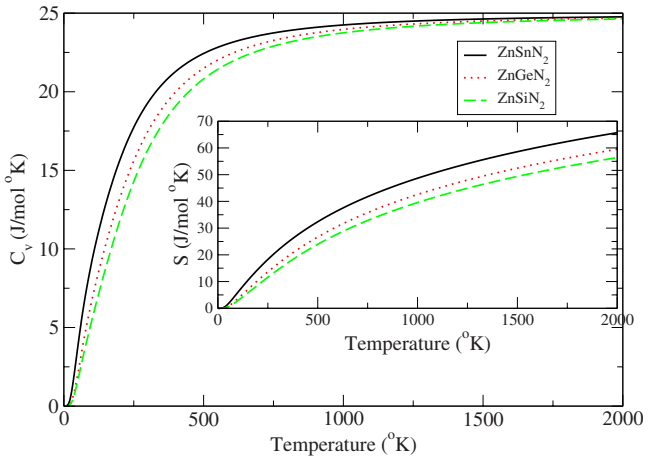

FIG. 12. (Color online) Specific heat at constant volume and entropy (inset) of the Zn-IV-N_2 compounds plotted against temperature.

tion geometries; (4) full phonon band dispersions along symmetry lines of the Brillouin zone; (5) phonon densities of states; and (6) integrated contributions of the phonons to the thermodynamic quantities such as Helmholtz free energy, average energy, specific heat, and entropy. Furthermore, quantities related to static long-range electric-field perturbations such as (1) Born effective charges and (2) high-frequency and static dielectric constants were also presented. Our discussion of structural properties includes lattice parameters, atomic positions in the cell, bond lengths, and bulk moduli.

The overall trends observed in the series are the expected ones: the lattice constants increase and the bonding weakens as we go from low to high atomic number Z for the IV element. Correspondingly, the phonon frequencies decrease. However, there are remarkable differences in the way the phonons are spread over mainly folded acoustic and mainly optic character frequency ranges. In particular, in $ZnSiN_2$ these ranges overlap so that it becomes difficult to assign a pure acoustic and pure optic region. We also find from the Born charges and other indications that $ZnSnN_2$ and $ZnSiN_2$ are somewhat more ionic in character than $ZnGeN_2$. This trend is the same as the corresponding trend in AlN, GaN, and InN, where GaN is the least ionic.

Most of the results presented here are predictions. Only a few experimental investigations exist: an infrared reflectivity study[16,17] of $ZnSiN_2$ that measured only the modes of one symmetry (the b_1 modes) and a Raman study[15] of $ZnGeN_2$ that only gave a complete assignment of the a_{1T} modes and some partial information on b_{2T} and densities of states. These were separately discussed in the citations indicated.

Although these materials are closely related to the III nitrides, their phonon related spectra are significantly more complex and cannot be understood simply in terms of folding of the modes in wurtzite plus small perturbations. The bimodal bond-length distribution and the complexity of having two types of cation masses significantly perturbs the phonons, which obtain an interesting mixed character with phonons spread out over much wider ranges than in the III nitrides.

ACKNOWLEDGMENTS

This work was supported by the Air Force Office of Scientific Research under Grant No. F49620-03-1-0010 and the Army Research Office under Grant No. W911NF-06-1-0476. The calculations were performed at the Core Facility in Advanced Research Computing of CWRU.

[1] S. J. Pearton, M. E. Overberg, C. R. Abernathy, N. A. Theodoropoulou, A. F. Hebard, S. N. G. Chu, A. Osinsky, V. Fuflyigin, L. D. Zhu, A. Y. Polyakov, and R. G. Wilson, J. Appl. Phys. **92**, 2047 (2002).

[2] K. Du, C. Bekele, C. C. Hayman, J. C. Angus, P. Pirouz, and K. Kash, J. Cryst. Growth **310**, 1057 (2008).

[3] K. Naniwae, S. Ithos, H. Amano, K. Hiramatsu, and I. Akasaki, J. Cryst. Growth **99**, 381 (1990).

[4] W. Larson, H. Maruska, and D. A. Stevenson, J. Electrochem. Soc. **121**, 1673 (1974).

[5] S. Kikkawa and H. Morisaka, Solid State Commun. **112**, 513 (1999).

[6] T. Endo, Y. Sato, H. Takizawa, and M. Shimada, J. Mater. Sci. Lett. **11**, 424 (1992).

[7] A. Osinsky, V. Fufluigin, L. D. Zhu, L. D. Goulakov, J. Graff, and E. Schubert, Proceedings of the 2000 IEEE/Cornell Conference on High Performance devices (IEEE, New York, 2000), pp. 168–172.

[8] J. Wu, W. Walukiewicz, K. M. Yu, J. W. Ager III, and E. E. Haller, Appl. Phys. Lett. **80**, 3967 (2002).

[9] T. R. Paudel and W. R. L. Lambrecht (unpublished).

[10] W. R. L. Lambrecht, in *Gallium Nitride (GaN) I*, Semiconductors and Semimetals Vol. 50, edited by J. I. Pankove and T. D. Moustakas (Academic, San Diego, 1998), Chap. 12, pp. 369–408.

[11] S. Limpijumnong, S. N. Rashkeev, and W. R. L. Lambrecht, MRS Internet J. Nitride Semicond. Res. **4S1**, G6.11 (1999).

[12] T. Misaki, X. Wu, A. Wakahara, and A. Yoshida, *Proceedings of the International Workshop on Nitride Semiconductors*, IPAP Conference Series Vol. 1 (The Institute of Pure and Applied Physics, Tokyo, 2000), pp. 685–688.

[13] V. L. Shaposhnikov, A. V. Krivosheeva, F. Arnaud D'Avitaya, J.-L. Lazzari, and V. E. Borisenko, Phys. Status Solidi B **245**, 142 (2008).

[14] W. R. L. Lambrecht, E. Alldredge, and K. Kim, Phys. Rev. B **72**, 155202 (2005).

[15] T. J. Peshek, T. R. Paudel, K. Kash, and W. R. L. Lambrecht, Phys. Rev. B **77**, 235213 (2008).

[16] T. R. Paudel and W. R. L. Lambrecht, Phys. Rev. B **76**, 115205 (2007).

[17] A. Mintairov, J. Merz, A. Osinsky, V. Fuflyigin, and L. Zhu, Appl. Phys. Lett. **76**, 2517 (2000).

[18] R. Viennois, T. Taliercio, V. Potin, A. Errebbahi, B. Gil, S. Charar, A. Haidoux, and J.-C. Tédenac, Mater. Sci. Eng., B **82**, 45 (2001).

[19] B. P. Cook, H. O. Everitt, I. Avrutsky, A. Osinsky, A. Cai, and J. F. Muth, Appl. Phys. Lett. **86**, 121906 (2005).

[20] S. Baroni, P. Giannozzi, and A. Testa, Phys. Rev. Lett. **58**, 1861 (1987).

[21] X. Gonze, Phys. Rev. B **55**, 10337 (1997).

[22] X. Gonze and C. Lee, Phys. Rev. B **55**, 10355 (1997).

[23] M. C. Payne, M. P. Teter, D. C. Allan, T. A. Arias, and J. D. Joannopoulos, Rev. Mod. Phys. **64**, 1045 (1992).

[24] P. Hohenberg and W. Kohn, Phys. Rev. **136**, B864 (1964).

[25] W. Kohn and L. J. Sham, Phys. Rev. **140**, A1133 (1965).

[26] X. Gonze, J. M. Beuken, R. Caracas, F. Detraux, M. Fuchs, G. M. Rignanese, M. Sindic, L. Verstraete, G. Zerah, and F. Jollet, Comput. Mater. Sci. **25**, 478 (2002); http://www.abinit.org.

[27] M. Veithen, X. Gonze, and P. Ghosez, Phys. Rev. B **71**, 125107 (2005).

[28] G. Deinzer and D. Strauch, Phys. Rev. B **66**, 100301(R) (2002).

[29] M. Fuchs and M. Scheffler, Comput. Phys. Commun. **119**, 67

(1999).
[30] C. Bungaro, K. Rapcewicz, and J. Bernholc, Phys. Rev. B **61**, 6720 (2000).
[31] M. Wintenberger, M. Maunaye, and Y. Laurent, Mater. Res. Bull. **8**, 1049 (1973).
[32] P. Vinet, J. Ferrante, J. R. Smith, and J. H. Rose, J. Phys. C **19**, L467 (1986).
[33] P. Y. Yu and M. Cardona, *Fundamental of Semiconductor* (Springer-Verlag, Berlin, 1999).
[34] C. Lee and X. Gonze, Phys. Rev. B **51**, 8610 (1995).
[35] V. Y. Davydov, V. V. Emtsev, I. N. Goncharuk, A. N. Smirnov, V. D. Petrikov, V. V. Mamutin, V. A. Vekshin, S. V. Ivanov, M. B. Smirnov, and T. Inushima, Appl. Phys. Lett. **75**, 3297 (1999).
[36] J. C. Nipko, C.-K. Loong, C. M. Balkas, and R. F. Davis, Appl. Phys. Lett. **73**, 34 (1998).
[37] V. Kosshchenko, Y. K. Grinberg, and A. Demidenko, Inorg. Mater. **20**, 1550 (1984).